8

On the Stability of Reduced-Order Linearized Computational Fluid Dynamics Models Based on POD and Galerkin Projection: Descriptor vs Non-Descriptor Forms

David Amsallem and Charbel Farhat

Abstract The Galerkin projection method based on modes generated by the Proper Orthogonal Decomposition (POD) technique is very popular for the dimensional reduction of linearized Computational Fluid Dynamics (CFD) models, among many other typically high-dimensional models in computational engineering. This, despite the fact that it cannot guarantee neither the optimality nor the stability of the Reduced-Order Models (ROMs) it constructs. Short of proposing any variant of this model order reduction method that guarantees the stability of its outcome, this paper contributes a best practice to its application to the construction of linearized CFD ROMs. It begins by establishing that whereas the solution snapshots computed using the descriptor and non-descriptor forms of the discretized Euler or Navier-Stokes equations are identical, the ROMs obtained by reducing these two alternative forms of the governing equations of interest are different. Focusing next on compressible fluid-structure interaction problems associated with computational aeroelasticity, this paper shows numerically that the POD-based fluid ROMs originating from the non-descriptor form of the governing linearized CFD equations tend to be unstable, but their counterparts originating from the descriptor form of these equations are typically stable and reliable for aeroelastic applications. Therefore, this paper argues that whereas many computations are performed in CFD codes using the non-descriptor form of discretized Euler and/or Navier-Stokes equations, POD-based model reduction in these codes should be performed using the descriptor form of these equations.

D. Amsallem (✉)
Department of Aeronautics and Astronautics, Durand Building, 496 Lomita Mall, Stanford University, Stanford, 94305-4035, USA
e-mail: amsallem@stanford.edu

C. Farhat
Department of Aeronautics and Astronautics, Department of Mechanical Engineering, and Institute for Computational & Mathematical Engineering, Durand Building, 496 Lomita Mall, Stanford University, Stanford, 94305-4035, USA
e-mail: cfarhat@stanford.edu

A. Quarteroni, G. Rozza (eds.): *Reduced Order Methods for Modeling and Computational Reduction*, MS&A 9. DOI 10.1007/978-3-319-02090-7_8,

8.1 Introduction

Linearized Computational Fluid Dynamics (CFD) models are ubiquitous in many applications pertaining to fluid dynamics. These include flow control, sensitivity analysis, shape optimization, flow stability analysis, and dynamic fluid-structure perturbation problems such as flutter, among others. In general, these computational models are less CPU intensive than their nonlinear counterparts. Nevertheless, because of the large dimensionality of these CFD models and the time-criticality of the aforementioned applications, there is a growing interest in developing Model Order Reduction (MOR) methods for constructing Reduced-Order Models (ROMs) that can capture the main characteristics of their high-dimensional counterparts at a fraction of the CPU cost they entail. A large class of such MOR methods is based on projection methods. These map a large number of degrees of freedom to a small number of generalized coordinates using a right Reduced-Order Basis (ROB). They also constrain the residual resulting from this approximation to be orthogonal to a left ROB.

The Proper Orthogonal Decomposition (POD) [27] – also known as the Singular Value Decomposition (SVD) – is a non-intrusive technique for generating a right ROB. Galerkin projections – that is, projections using identical left and right ROBs – with POD "modes" constitute a popular mean for constructing CFD-based linear ROMs [1,2,5,11,14,23,29]. This, despite the fact this approach for model reduction does not guarantee neither the optimality nor the stability of the ROMs it produces. To address the issue of ROMs constructed without a guaranteed stability, stabilization methods [4, 6] have been developed. In the specific context of CFD applications, more intrusive POD-based techniques have also been successfully developed for MOR. As it can be expected, each of these alternative approaches for restoring or guaranteeing stability has advantages and shortcomings.

Alternatively, this paper sheds some light on the behavior of the basic POD-based Galerkin projection method for CFD applications. It also proposes a best practice for reducing the occurrence of unstable POD-based linear ROMs that has proved to be effective for a large number of CFD problems. It conjectures that a large number of these occurrences is promoted by the application of the reduction process to the non-descriptor form [24] of the governing CFD equations. This form of an Ordinary Differential Equation (ODE) (or a set of them), which is also known as the "autonomous form of an ODE system," is characterized by the identity matrix as the coefficient of the term with the highest derivative. It is popular in many computational engineering applications including multibody dynamics [15, 17], molecular dynamics [26], and CFD [2,7,16,20,23]. This paper also shows numerically that, on the other hand, when MOR is applied to the descriptor form [24] of the governing equations, stable CFD ROMs are typically obtained.

To this effect, the remainder of this paper is organized as follows. Section 8.2 sets the stage for linearized Arbitrary Lagrangian Eulerian (ALE) CFD problems with moving boundaries and their semi-discretization by a finite volume method. The emphasis on moving boundaries is due to their predominant role in generating unsteady flows – even in the absence of turbulence – and their importance in dynamic fluid-

structure applications. This section also introduces the descriptor and non-descriptor forms of a Linear Time-Invariant (LTI) system. Section 8.3 overviews the POD-based Galerkin projection model in the context of linearized CFD problems. More specifically, it shows that whereas the snapshot solutions computed using either the descriptor or non-descriptor form of a CFD-based LTI system are identical, the linear ROMs obtained by reducing both forms of this system using a Galerkin projection method are different. Section 8.4 focuses on realistic dynamic fluid-structure interaction problems to illustrate the formulated conjecture. It also highlights the robustness of Galerkin projections with POD modes when applied to the descriptor form of the governing fluid equations. Finally, Sect. 8.5 summarizes and this paper and concludes it.

8.2 Linearized CFD-Based Analysis

8.2.1 Governing Equations in Descriptor Form

The semi-discretization of the ALE form of the Navier-Stokes equations with moving boundaries by a finite volume method leads to the following system of ODEs

$$\dot{(\widehat{\mathbf{V}(\mathbf{x})\mathbf{w}})} + \mathbf{F}(\mathbf{w}, \mathbf{x}, \dot{\mathbf{x}}) = \mathbf{0}, \tag{8.1}$$

where:

- a dot denotes the derivative with respect to time t;
- $\mathbf{V} \in \mathbb{R}^{N_f \times N_f}$ is a diagonal matrix storing the cell volumes and N_f denotes the dimension of the semi-discrete fluid system;
- $\mathbf{w}(t) \in \mathbb{R}^{N_f}$ denotes the time-dependent conservative fluid state vector;
- $\mathbf{F} \in \mathbb{R}^{N_f}$ denotes the vector of numerical fluxes;
- $\mathbf{x}$ denotes the vector position of the CFD mesh nodes.

The linearization of (8.1) about an equilibrium state $(\mathbf{w}_0, \mathbf{x}_0, \dot{\mathbf{x}}_0)$ designated by the subscript 0 leads to the following set of ODEs [21]

$$\mathbf{V}_0 \delta\dot{\mathbf{w}} + \mathbf{H}_0 \delta\mathbf{w} + \mathbf{R}_0 \delta\dot{\mathbf{x}} + \mathbf{G}_0 \delta\mathbf{x} = \mathbf{0}, \tag{8.2}$$

where:

- δ designates a small perturbation of the quantity it is applied to;
- The subscript 0 designates the evaluation of a quantity at the equilibrium state $(\mathbf{w}_0, \mathbf{x}_0, \dot{\mathbf{x}}_0)$;
- $\mathbf{H}_0 = \left.\dfrac{\partial \mathbf{F}}{\partial \mathbf{w}}\right|_0 \in \mathbb{R}^{N_f \times N_f}$ denotes the Jacobian of the vector of numerical fluxes with respect to $\mathbf{w}$, at the equilibrium state $(\mathbf{w}_0, \mathbf{x}_0, \dot{\mathbf{x}}_0)$;
- $\mathbf{R} = \mathbf{E}_0 + \left.\frac{\partial \mathbf{F}}{\partial \dot{\mathbf{x}}}\right|_0 \in \mathbb{R}^{N_f \times N_f}$, where, using Einstein's notation, $E_{0_{ij}} = \left.\frac{\partial A_{il}}{\partial x_j}\right|_0 w_{0_l}$ denotes the Jacobian of the vector of numerical fluxes with respect to $\dot{\mathbf{x}}$, at the equilibrium state $(\mathbf{w}_0, \mathbf{x}_0, \dot{\mathbf{x}}_0)$;

- $\mathbf{G} = \left.\frac{\partial \mathbf{F}}{\partial \mathbf{x}}\right|_0 \in \mathbb{R}^{N_f \times N_f}$ denotes the Jacobian of the vector of numerical fluxes with respect to $\mathbf{x}$, at the equilibrium state $(\mathbf{w}_0, \mathbf{x}_0, \dot{\mathbf{x}}_0)$.

To keep the notation as simple as possible, the symbold δ and the subscript 0 are dropped throughout the remainder of this paper. Hence, Eq. (8.2) is re-written as

$$\mathbf{V}\dot{\mathbf{w}} + \mathbf{H}\mathbf{w} + \mathbf{R}\dot{\mathbf{x}} + \mathbf{G}\mathbf{x} = \mathbf{0}. \tag{8.3}$$

Equation (8.3) above is said to be in "descriptor" form because $\mathbf{V} \neq \mathbf{I}_{N_f}$, where $\mathbf{I}_{N_f}$ denotes the identity matrix of dimension N_f. Equation (8.3) is also referred to here as a LTI system because all matrices $\mathbf{V}$, $\mathbf{H}$, $\mathbf{R}$, and $\mathbf{G}$ are time-independent.

The reader is reminded that the leading matrix $\mathbf{V}$ is diagonal and that its entries store the volumes of the cells of the CFD mesh. For external flow problems around rigid or flexible bodies, the cells are usually very small near the wall boundaries, and very large near the far-field artificial boundaries. Hence for such CFD problems, $\mathbf{V}$ is diagonal but ill-conditioned.

8.2.2 Governing Equations in Non-Descriptor Form

The nonlinear equations (8.1) can also be written as

$$\mathbf{r}(\mathbf{w}, \mathbf{x}, \dot{\mathbf{x}}) = \mathbf{0}, \tag{8.4}$$

where

$$\mathbf{r}(\mathbf{w}, \mathbf{x}, \dot{\mathbf{x}}) = \mathbf{V}(\mathbf{x})\dot{\mathbf{w}} + \dot{\mathbf{V}}(\mathbf{x})\mathbf{w} + \mathbf{F}(\mathbf{w}, \mathbf{x}, \dot{\mathbf{x}}). \tag{8.5}$$

Hence, given an iterate fluid state vector $(\mathbf{w}^k, \mathbf{x}^k, \dot{\mathbf{x}}^k)$, $\mathbf{r}(\mathbf{w}^k, \mathbf{x}^k, \dot{\mathbf{x}}^k)$ designates the residual associated with it – that is, the residual associated with a k-th iteration applied to the solution of Eq. (8.4).

Consider next the scaled residual

$$\tilde{\mathbf{r}}(\mathbf{w}, \mathbf{x}, \dot{\mathbf{x}}) = \mathbf{V}^{-1}(\mathbf{x})\mathbf{r}(\mathbf{w}, \mathbf{x}, \dot{\mathbf{x}}). \tag{8.6}$$

From a purely numerical analysis viewpoint, it could be argued that scaling $\mathbf{r}$ by $\mathbf{V}^{-1}$ is a bad idea because it involves the multiplication of the governing nonlinear equations of equilibrium (8.1) by the inverse of a matrix. However, in both steady and unsteady CFD codes, it is common practice to work with the scaled residual introduced above for the following reasons:

- scaling the entries of $\mathbf{r}$ by the corresponding inverses of the cell volumes magnifies the residual in the small cells. In this case, given a stopping criterion and a convergence tolerance, the solution of Eq. (8.4) delivered by a finite number of iterations is most accurate in the flow regions where the cells are the smallest. This is highly desirable because the smallest cells are typically located in the flow regions where accuracy is most sought-after in the first place;
- after time-discretization, scaling the entries of $\mathbf{r}$ by the corresponding inverses of the cell volumes accelerates the convergence of an iterative process based on local time-stepping and applied to the steady-state solution of Eq. (8.3) [18];

- since $\mathbf{V}$ is diagonal, inverting this matrix is trivial.

The scaling (8.6) is associated with the following nonlinear semi-discrete fluid equations of equilibrium

$$\mathbf{I}_{N_f}\dot{\mathbf{w}} + \mathbf{V}^{-1}\dot{\mathbf{V}}(\mathbf{x})\mathbf{w} + \mathbf{V}^{-1}\mathbf{F}(\mathbf{w}, \mathbf{x}, \dot{\mathbf{x}}) = \mathbf{0}. \tag{8.7}$$

The linearization of these equations about the equilibrium state $(\mathbf{w}_0, \mathbf{x}_0, \dot{\mathbf{x}}_0)$ leads to

$$\mathbf{I}_{N_f}\dot{\mathbf{w}} + \mathbf{V}^{-1}\mathbf{H}\mathbf{w} + \mathbf{V}^{-1}\mathbf{R}\dot{\mathbf{x}} + \mathbf{V}^{-1}\mathbf{G}\mathbf{x} = \mathbf{0}. \tag{8.8}$$

Equation (8.8) above is said to be in "non-descriptor" form, because the matrix coefficient of its leading term (or term with the highest derivative) is the identity matrix $\mathbf{I}_{N_f}$. This LTI system is mathematically equivalent to its counterpart (8.3) which is written in descriptor form.

It is conjectured here that because the non-descriptor form (8.7) of the nonlinear semi-discrete fluid equations of equilibrium prevails in many CFD codes, POD-based model reduction is performed in some if not many of these codes using either inadvertently or purposely the non-descriptor form (8.8) of the governing linearized semi-discrete fluid equations of equilibrium. For example, this is the case for the POD-based model reductions performed in [20], [23], [2], [16], and [7]. For this reason, one objective of this paper is to analyze the differences, if any, between the linear ROMs constructed by reducing the descriptor form of the governing equations (8.3), and their counterparts constructed by reducing the non-descriptor form (8.8) of these equations.

8.3 Model Order Reduction via Galerkin Projection Based on POD Modes

Whether applied to the descriptor or non-descriptor form of a LTI fluid system, a projection-based MOR method generates another LTI fluid system of much smaller dimension $k_f << N_f$. In general, such a MOR method operates using two ROBs:

- a right (or trial) ROB $\Phi \in \mathbb{R}^{N_f \times k_f}$ which has full-column rank and is introduced to approximate the state vector $\mathbf{w}(t)$ as follows:

$$\mathbf{w}(t) \approx \Phi \mathbf{w}_r(t). \tag{8.9}$$

  In this case, the approximate state vector is uniquely defined by the vector of generalized coordinates $\mathbf{w}_r \in \mathbb{R}^{k_f}$. Substituting this approximation into the LTI fluid system of interest yields a non-zero residual $\mathbf{r}(t) \in \mathbb{R}^{N_f}$;
- a left (or test) ROB $\Psi \in \mathbb{R}^{N_f \times k_f}$ which also has full-column rank, and is introduced to limit the magnitude of the residual $\mathbf{r}(t)$ by constraining it to satisfy the orthogonality condition $\Psi^T \mathbf{r}(t) = \mathbf{0}$, where the superscript T designates the transpose.

When $\Psi \neq \Phi$, a projection-based MOR method is also known as a Petrov-Galerkin approximation method. When $\Psi = \Phi$, it is known as a Galerkin approximation method.

In the remainder of this paper, the focus is set on the Galerkin projection method ($\Psi = \Phi$), and the POD technique for constructing the ROB Φ.

8.3.1 Snapshot Collection

The POD technique based on numerical snapshots [27] computes a trial ROB Φ by compressing the information contained in solution snapshots of the system of interest. For LTI systems, these snapshots can be computed either in the time domain, or in the frequency domain. To simplify notation, only the case of a single forcing input function $\mathbf{x}(t)$ is presented below. However, it is noted that the extension to multiple inputs is straightforward (for example, see [23]).

In the time domain, solution snapshots are obtained by computing the dynamic response of the LTI system of interest to a given impulse forcing input and collecting samples of the time-dependent response $\{\mathbf{w}(t_i)\}_{i=1}^{N_w}$, where N_w denotes the number of snapshots, in a matrix $\mathbf{W}$ as follows

$$\mathbf{W} = \mathbf{W}(t_1, \cdots, t_{N_w}) = \left[\mathbf{w}(t_1) \ \ldots \ \mathbf{w}(t_{N_w})\right]. \tag{8.10}$$

In the frequency domain, complex-valued snapshots [19, 22, 23, 28, 30] are obtained by formulating and solving the dynamic response problem in the frequency domain, and collecting samples of the frequency-dependent response in a similar matrix $\mathbf{W}$. For example, when working with the LTI system (8.3) written in descriptor form, the following frequency domain problems are formulated and solved

$$(j\omega_i \mathbf{V} + \mathbf{H})\mathbf{w}(\omega_i) = -(j\omega_i \mathbf{R} + \mathbf{G})\mathbf{x}, \qquad i = 1, 2, \cdots, N_w, \tag{8.11}$$

where ω_i denotes a sampled circular frequency of interest, j denotes the pure imaginary complex number satisfying $j^2 = -1$, and $\mathbf{x}$ denotes the amplitude of a harmonic mesh motion driven by a harmonic displacement of the body around which the flow is computed. Then, the computed complex-valued samples $\mathbf{w}(\omega_i)$ are collected in a snapshot matrix $\mathbf{W}$ as follows

$$\mathbf{W} = \mathbf{W}(\omega_1, \cdots, \omega_{N_w}) = \left[\mathrm{Re}\,(\mathbf{w}(\omega_1)) \ldots \mathrm{Re}\,(\mathbf{w}(\omega_{N_w}))\, \mathrm{Im}\,(\mathbf{w}(\omega_1)) \ldots \mathrm{Im}\,(\mathbf{w}(\omega_{N_w}))\right]. \tag{8.12}$$

Similarly, when working with the LTI fluid system (8.8) written in non-descriptor form, the frequency domain problems are formulated as follows

$$(j\omega_i \mathbf{I}_{N_f} + \mathbf{V}^{-1}\mathbf{H})\mathbf{w}(\omega_i) = -(j\omega_i \mathbf{V}^{-1}\mathbf{R} + \mathbf{V}^{-1}\mathbf{G})\mathbf{x}, \qquad i = 1, 2, \cdots, N_w, \tag{8.13}$$

and the computed complex-valued samples $\mathbf{w}(\omega_i)$ are collected in a similar snapshot matrix $\mathbf{W}$ as above.

At this point, it is noted that whether collected in the time or frequency domain, and except for round-off effects, the snapshots are independent of the form

in which the underlying LTI system is written. This is because both descriptor and non-descriptor forms of a LTI system are mathematically equivalent. However, as it will be shown below, the trial ROBs Φ constructed using these snapshots differ.

8.3.2 Reduction of the Descriptor Form of the Governing Equations

Suppose that the LTI fluid system written in descriptor form (8.3) is chosen as the computational fluid model of interest. Note that the diagonal matrix $\mathbf{V}$ is also a symmetric positive definite matrix and therefore defines a norm. Hence in this case, after all solution snapshots are computed in either the time or frequency domain, the POD technique proceeds with performing the eigenvalue decomposition

$$\mathbf{W}^T\mathbf{V}\mathbf{W} = \hat{\mathbf{U}}^d\hat{\Lambda}^d\hat{\mathbf{U}}^{dT}, \tag{8.14}$$

where $\mathbf{W}^T\mathbf{V}\mathbf{W} \in \mathbb{R}^{N_w \times N_w}$ is usually a small-size matrix, and the superscript d designates the descriptor form of the underlying governing equations. Next, this decomposition is truncated to account only for the first k_f eigenvalues of $\hat{\Lambda}^d$ and their corresponding eigenvectors, and the trial ROB Φ^d is constructed as follows

$$\Phi^d = \mathbf{W}\mathbf{U}^d\Lambda^{d^{-\frac{1}{2}}}, \tag{8.15}$$

where $\mathbf{U}^d$ and Λ^d are the truncated counterparts of $\hat{\mathbf{U}}^d$ and $\hat{\Lambda}^d$, respectively.

Alternatively, Φ^d can be constructed by first computing the SVD of the matrix $\mathbf{V}^{\frac{1}{2}}\mathbf{W}$, retaining the first k_f left singular vectors $\mathbf{Y}$, and finally performing the following matrix-matrix multiplication

$$\Phi^d = \mathbf{V}^{-\frac{1}{2}}\mathbf{Y}. \tag{8.16}$$

Finally, performing a Galerkin projection of the governing equations (8.3) using $\Psi = \Phi = \Phi^d$ leads to the reduced-order LTI fluid system

$$\dot{\mathbf{w}}_r + \left(\Phi^{dT}\mathbf{H}\Phi^d\right)\mathbf{w}_r + \left(\Phi^{dT}\mathbf{R}\right)\dot{\mathbf{x}} + \left(\Phi^{dT}\mathbf{G}\right)\mathbf{x} = \mathbf{0}, \tag{8.17}$$

which is also referred to here as the linear fluid ROM based on the descriptor form of the governing equations.

8.3.3 Reduction of the Non-Descriptor Form of the Governing Equations

If on the other hand the non-descriptor form (8.8) of the LTI system of interest is chosen as the computational model of interest, the POD process proceeds with performing the following eigen decomposition instead

$$\mathbf{W}^T\mathbf{W} = \hat{\mathbf{U}}^{nd}\hat{\Lambda}^{nd}\hat{\Phi}^{ndT}, \tag{8.18}$$

where the superscript nd designates the non-descriptor form of the underlying equations, and Φ^{nd} is constructed as in (8.15). Then, performing a Galerkin projection

of the governing equations (8.8) using this trial ROB leads to

$$\dot{\mathbf{w}}_r + \left(\boldsymbol{\Phi}^{nd^T}\mathbf{V}^{-1}\mathbf{H}\boldsymbol{\Phi}^{nd}\right)\mathbf{w}_r + \left(\boldsymbol{\Phi}^{nd^T}\mathbf{V}^{-1}\mathbf{R}\right)\dot{\mathbf{x}} + \left(\boldsymbol{\Phi}^{nd^T}\mathbf{V}^{-1}\mathbf{G}\right)\mathbf{x} = \mathbf{0}. \quad (8.19)$$

This reduced LTI fluid system is also referred to here as the linear fluid ROM based on the non-descriptor form of the governing equations.

8.3.4 Comparison of Alternative Reduced-Order Models

From (8.14) and (8.18), if follows that for $\mathbf{V} \neq \mathbf{I}_{N_f}$, $\mathbf{U}^d \neq \mathbf{U}^{nd}$, and therefore $\boldsymbol{\Phi}^d \neq \boldsymbol{\Phi}^{nd}$. Hence, the linear fluid ROM (8.17) based on the descriptor form of the governing equations is in general different from its counterpart (8.19) based on the non-descriptor form of the governing equations.

Remark. The reader can check that if the descriptor form of the LTI fluid system of interest is reduced by a Galerkin projection method, but its non descriptor form is reduced instead by a Petrov-Galerkin method, the choices

$$\boldsymbol{\Phi}^{nd} = \boldsymbol{\Phi}^d, \quad \boldsymbol{\Psi}^d = \boldsymbol{\Phi}^d, \quad \text{and} \quad \boldsymbol{\Psi}^{nd} = \mathbf{V}\boldsymbol{\Phi}^d \quad (8.20)$$

lead to two linear fluid ROMs that are identical. However, the focus of this work is set exclusively on the popular Galerkin projection method, and on the POD modes.

8.4 Applications to Dynamic Fluid-Structure Interaction Problems

Now that it has been established that the reductions of the descriptor and non-descriptor forms of a LTI system by a Galerkin projection method lead to two different ROMs, it remains to assess whether in the case where the ROBs are generated using the POD technique, the two alternative ROMs exhibit or not different accuracy and numerical stability properties for interesting applications. This is the objective of this section which, for this purpose, focuses on a special class of fluid-structure interaction problems known as aeroelasticity. Such problems are usually characterized by a linear, elastic structural subsystem, and a high-speed compressible fluid subsystem. The present focus on aeroelastic applications is motivated by the fact that linearized CFD is rapidly becoming a very competitive approach for modeling the fluid component of a perturbed aeroelastic system, primarily because it provides a relatively low-cost mean for capturing the effects of shocks in the transonic regime.

To this effect, each of the two fluid ROMs developed in Sectsions 8.3.2 and 8.3.3 is coupled here with a classical modal ROM of the structural subsystem past which the flow is computed, in order to obtain in each case a linear fluid-structure ROM. Then, two *inviscid* aeroelastic applications are considered: the flutter analysis in transonic air speeds of a wing-store-fuel configuration and of a F/A-18 fighter jet configuration, respectively. For each application, the numerical stability of the fluid ROM constructed using the descriptor or non-descriptor form of the governing fluid equa-

tions is assessed, and its effect on the behavior of the corresponding coupled fluid-structure ROM is highlighted.

8.4.1 Linearized Coupled Fluid-Structure Reduced-Order Models

CFD-based linearized computational fluid models are rapidly becoming the preferred computational models for representing the behavior of a compressible fluid subsystem in a coupled fluid-structure system. For example, they are very popular nowadays in aeronautics for the flutter analysis of modern aircraft in the transonic and other nonlinear regimes [10, 21, 25], and for loads analysis. In this and many other related contexts, the structural subsystem of interest is typically represented by a linearized finite element model that can be described by the following set of linear ODEs

$$\mathbf{M}\ddot{\mathbf{u}} + \mathbf{D}\dot{\mathbf{u}} + \mathbf{K}\mathbf{u} = \sqrt{p_\infty}\mathbf{P}\mathbf{w}, \tag{8.21}$$

where $\mathbf{u} \in \mathbb{R}^{N_s}$ denotes the vector of structural displacements of dimension N_s, $\mathbf{M} \in \mathbb{R}^{N_s \times N_s}$, $\mathbf{D} \in \mathbb{R}^{N_s \times N_s}$ and $\mathbf{K} \in \mathbb{R}^{N_s \times N_s}$ are the finite element structural mass, damping, and stiffness matrices, respectively, p_∞ is the free-stream pressure, and $\mathbf{P} \in \mathbb{R}^{N_s \times N_f}$ denotes the Jacobian of the aerodynamic forces acting on the wet surface of the structure with respect to the fluid state vector $\mathbf{w}$. The reader is reminded that in this work, all vector quantities appearing in a linearized context are perturbations and that the symbold δ is dropped to keep the notation as simple as possible (see Sect. 8.2.1).

Modal decomposition is perhaps the most popular MOR method for a LTI structural subsystem such as that described in Eq. (8.21). In this case, the ROB $\mathbf{X} \in \mathbb{R}^{N_s \times k_s}$ is constructed using the first k_s natural mode shapes of the structural subsystem, and Eq. (8.21) is reduced by a Galerkin projection onto the subspace of dimension k_s spanned by the columns of $\mathbf{X}$. In other words, $\mathbf{u}(t)$ is approximated as follows

$$\mathbf{u}(t) \approx \mathbf{X}\mathbf{u}_r(t), \tag{8.22}$$

where $\mathbf{u}_r \in \mathbb{R}^{k_s}$ is the vector of generalized (modal) coordinates, and Eq. (8.21) is transformed into the following linear structural ROM

$$\ddot{\mathbf{u}}_r + \mathbf{D}_r\dot{\mathbf{u}}_r + \Omega_r^2\mathbf{u}_r = \sqrt{p_\infty}\mathbf{P}_r\mathbf{w}_r, \tag{8.23}$$

where

$$\mathbf{D}_r = \mathbf{X}^T\mathbf{D}\mathbf{X}, \quad \mathbf{P}_r = \mathbf{X}^T\mathbf{P}\boldsymbol{\Phi}, \tag{8.24}$$

$\boldsymbol{\Phi} = \boldsymbol{\Phi}^d$ if the descriptor form of the LTI fluid subsystem is reduced, or $\boldsymbol{\Phi} = \boldsymbol{\Phi}^{nd}$ if the non-descriptor form of the LTI fluid subsystem is reduced, and $\Omega_r \in \mathbb{R}^{k_s \times k_s}$ is the diagonal matrix of natural circular frequencies of the structure.

Assimilating the ALE fluid mesh with a quasi-static pseudo-structure [9, 12] and enforcing the compatibility of the displacements of the structural subsystem and the ALE fluid mesh across the wet surface of the structure results in a linear relationship between $\mathbf{x}$ and $\mathbf{u}$ that can be written as [21]

$$\mathbf{x} = \mathbf{K}^\star\mathbf{u}, \tag{8.25}$$

where $\mathbf{K}^\star$ is a time-independent operator described in [13, 21]. Hence, substituting the above relationship into the LTI fluid subsystem written in descriptor form (8.3) yields

$$\mathbf{V}\dot{\mathbf{w}} + \mathbf{H}\mathbf{w} + \mathbf{R}\mathbf{K}^\star\dot{\mathbf{u}} + \mathbf{G}\mathbf{K}^\star\mathbf{u} = \mathbf{0}, \tag{8.26}$$

and substituting it into the LTI fluid subsystem written in non-descriptor form (8.8) yields

$$\dot{\mathbf{w}} + \mathbf{V}^{-1}\mathbf{H}\mathbf{w} + \mathbf{V}^{-1}\mathbf{R}\mathbf{K}^\star\dot{\mathbf{u}} + \mathbf{V}^{-1}\mathbf{G}\mathbf{K}^\star\mathbf{u} = \mathbf{0}. \tag{8.27}$$

Let

$$\mathbf{H} = \sqrt{\frac{p_\infty}{\rho_\infty}}\bar{\mathbf{H}} \quad \text{and} \quad \mathbf{G} = \sqrt{\frac{p_\infty}{\rho_\infty}}\bar{\mathbf{G}}, \tag{8.28}$$

where ρ_∞ denotes the free-stream density, and $\bar{\mathbf{H}}$ and $\bar{\mathbf{G}}$ do not depend neither on the free-stream pressure p_∞ nor on ρ_∞ [22, 23], but only on the free-stream Mach number M_∞.

Substituting the above expressions of $\mathbf{H}$ and $\mathbf{G}$ into Eq. (8.26) and Eq. (8.27) leads in the descriptor case to

$$\mathbf{V}\dot{\mathbf{w}} + \sqrt{\frac{p_\infty}{\rho_\infty}}\bar{\mathbf{H}}\mathbf{w} + \mathbf{R}\mathbf{K}^\star\dot{\mathbf{u}} + \sqrt{\frac{p_\infty}{\rho_\infty}}\bar{\mathbf{G}}\mathbf{K}^\star\mathbf{u} = \mathbf{0}, \tag{8.29}$$

and in the non-descriptor case to

$$\dot{\mathbf{w}} + \sqrt{\frac{p_\infty}{\rho_\infty}}\mathbf{V}^{-1}\bar{\mathbf{H}}\mathbf{w} + \mathbf{V}^{-1}\mathbf{R}\mathbf{K}^\star\dot{\mathbf{u}} + \sqrt{\frac{p_\infty}{\rho_\infty}}\mathbf{V}^{-1}\bar{\mathbf{G}}\mathbf{K}^\star\mathbf{u} = \mathbf{0}. \tag{8.30}$$

Next, reducing the LTI fluid subsystems (8.29) and (8.30) by the Galerkin projection method based on Φ^d and Φ^{nd}, respectively, leads to the following general expression of the linear fluid ROM

$$\dot{\mathbf{w}}_r + \sqrt{\frac{p_\infty}{\rho_\infty}}\mathbf{H}_r\mathbf{w}_r + \mathbf{R}_r\dot{\mathbf{u}}_r + \sqrt{\frac{p_\infty}{\rho_\infty}}\mathbf{G}_r\mathbf{u}_r = \mathbf{0} \tag{8.31}$$

where

$$\mathbf{H}_r = \Phi^{d^T}\bar{\mathbf{H}}\Phi^d, \quad \mathbf{R}_r = \Phi^{d^T}\mathbf{R}\mathbf{K}^\star\mathbf{X}, \quad \mathbf{G}_r = \Phi^{d^T}\bar{\mathbf{G}}\mathbf{K}^\star\mathbf{X} \tag{8.32}$$

in the descriptor case, and

$$\mathbf{H}_r = \Phi^{nd^T}\mathbf{V}^{-1}\bar{\mathbf{H}}\Phi^{nd}, \quad \mathbf{R}_r = \Phi^{nd^T}\mathbf{V}^{-1}\mathbf{R}\mathbf{K}^\star\mathbf{X}, \quad \mathbf{G}_r = \Phi^{nd^T}\mathbf{V}^{-1}\mathbf{G}\bar{\mathbf{K}}^\star\mathbf{X} \tag{8.33}$$

in the non-descriptor case.

Finally, re-writing Eq. (8.23) in first-order form and combining it with Eq. (8.31) leads to the following coupled fluid-structure linear ROM of dimension $k_f + 2k_s$

$$\begin{bmatrix} \dot{\mathbf{w}}_r \\ \ddot{\mathbf{u}}_r \\ \dot{\mathbf{u}}_r \end{bmatrix} = \begin{bmatrix} -\sqrt{\frac{p_\infty}{\rho_\infty}}\mathbf{H}_r & -\mathbf{R}_r & -\sqrt{\frac{p_\infty}{\rho_\infty}}\mathbf{G}_r \\ \sqrt{p_\infty}\mathbf{P}_r & -\mathbf{D}_r & -\Omega_r^2 \\ \mathbf{0} & \mathbf{I}_{k_s} & \mathbf{0} \end{bmatrix} \begin{bmatrix} \mathbf{w}_r \\ \dot{\mathbf{u}}_r \\ \mathbf{u}_r \end{bmatrix}. \tag{8.34}$$

This ROM can be used for several fluid-structure applications ranging from real-time control to real-time flutter analysis. In the latter case, the onset of flutter at a given

free-stream Mach number M_∞ can be established by fixing the free-stream density ρ_∞ and increasing the free-stream pressure p_∞ until this coupled fluid-structure ROM becomes unstable. At this point, the free-stream pressure p_∞ reaches a critical value denoted here by p_∞^{cr}. This fast approach to flutter analysis requires however that the ROM (8.34) be stable outside the flutter point. In [4], it was shown that this in turn requires that the reduced fluid matrix $\mathbf{H}_r$ be stable. Hence, the application of the linear ROM (8.34) to the flutter analysis of a coupled fluid-structure system highlights the importance of requiring the chosen MOR method to preserve the stability of the LTI system or subsystem to which it is applied (for example, see [4]).

8.4.2 Flutter Analysis of a Wing-Store-Fuel Configuration

Consider first the wing-store-fuel aeroelastic configuration described in [8] and graphically depicted in Fig. 8.1. For a fixed altitude characterized by specific values of the free-stream pressure p_∞ and density ρ_∞, a flight condition for this configuration is defined here by an additional pair of data values corresponding to the free-stream Mach number M_∞ and fuel fill level in the store (or tank). The hydroelastic effects due to the presence of fuel inside the tank modify the structural properties of the system and affect its aeroelastic characteristics. The High-Dimensional computational fluid and structural Models (HDMs) developed in [8] for this aeroelastic configuration have the dimensions $N_f = 689,485$ and $N_s = 6,834$, respectively.

For every flight condition of interest, 44 real-valued fluid snapshots are generated by exciting the wall boundary of the structural system by each of its first $k_s = 4$ structural mode shapes at each of six equispaced reduced frequencies in the interval $[0, 0.0125]$. Then, these snapshots are compressed by the POD technique to construct a suite of fluid ROBs of dimension $k_f \in \{1, \cdots, 40\}$. A corresponding suite of fluid ROMs of the same dimension k_f is also constructed by performing Galerkin projections of both descriptor and non-descriptor forms of the LTI fluid subsystem onto these ROBs.

In all cases, the structural ROM is constructed as in (8.23) with $k_s = 4$ and rewritten in first-order form.

Fig. 8.1. High-dimensional aeroelastic model of a wing-store configuration. (a) CFD surface grid; (b) Finite element structural model

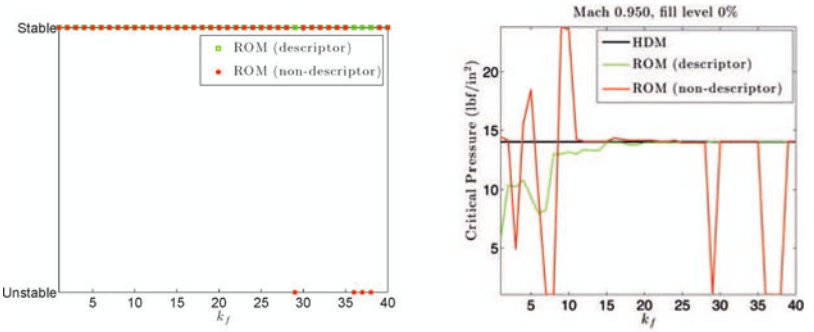

(a) Stability (b) Accuracy

Fig. 8.2. Wing-store-fuel configuration ($M_\infty = 0.95$ and empty tank): stability of the fluid ROM as a function of its dimension, and accuracy of the critical free-stream pressure predicted using the corresponding aeroelastic ROM

The first considered flight condition is defined by $M_\infty = 0.95$ and an empty tank. In this case, Figure 8.2(a) reports on the stability of the constructed fluid ROMs – that is, the stability of the matrices $\mathbf{H}_r$. Figure 8.2(b) reports on the accuracy they deliver for the prediction of the critical pressure. All fluid ROMs originating from the descriptor form of the LTI fluid subsystem are found to be stable. On the other hand, the fluid ROMs of dimension $k_f \in \{29, 36, 37, 38\}$ originating from the non-descriptor form of the LTI fluid subsystem are found to be unstable. Consequently, each unstable fluid ROM leads to an erroneous prediction of the critical pressure using the coupled fluid-structure ROM (8.34) (see Fig. 8.2(b)). In contrast, all fluid-structure ROMs of dimension $k_f \geq 15$ originating from the descriptor form of the LTI fluid subsystem deliver accurate predictions of the critical pressure. Similar results were also reported in [3] where a preliminary study of this problem was first performed.

The second and third considered flight conditions are defined by $M_\infty = 1.1$ and 31% fuel fill level in the tank, and $M_\infty = 0.75$ and 69% fuel fill level, respectively. Figures 8.3 and 8.4 report on the stability of the constructed fluid ROMs and accuracy of the corresponding aeroelastic ROMs for these two cases, respectively. These figures confirm the trends observed for the first flight condition and lead to similar conclusions.

8.4.3 Flutter Analysis of an F/A-18 Aircraft Configuration

Next, an aeroelastic HDM of a full F/A-18 configuration with tip missiles is considered (see Fig. 8.5). Here, the dimension of the fluid HDM is $N_f = 1{,}054{,}500$, and that of the structural HDM is $N_s = 9{,}046$. The latter is reduced by Galerkin projection on a modal basis with $k_s = 10$ flexible structural mode shapes.

The free-stream condition is set to $M_\infty = 0.99$. Then, 210 fluid snapshots are computed in the frequency domain by exciting the wall boundary of the aircraft configuration using all 10 structural modal displacements individually, each at 21

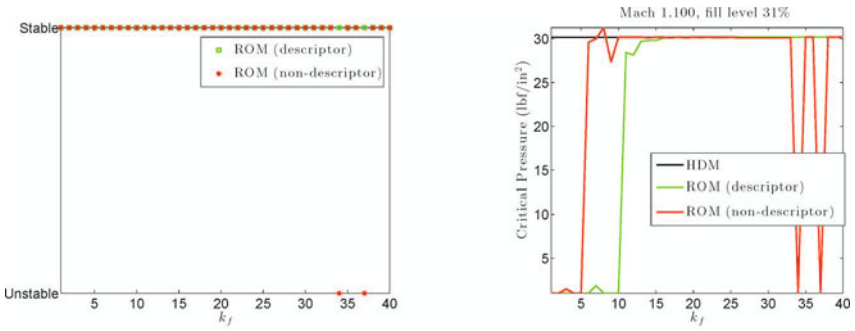

(a) Stability (b) Accuracy

Fig. 8.3. Wing-store-fuel configuration ($M_\infty = 1.1$ and 31% fuel fill level): stability of the fluid ROM as a function of its dimension, and accuracy of the critical free-stream pressure predicted using the corresponding aeroelastic ROM

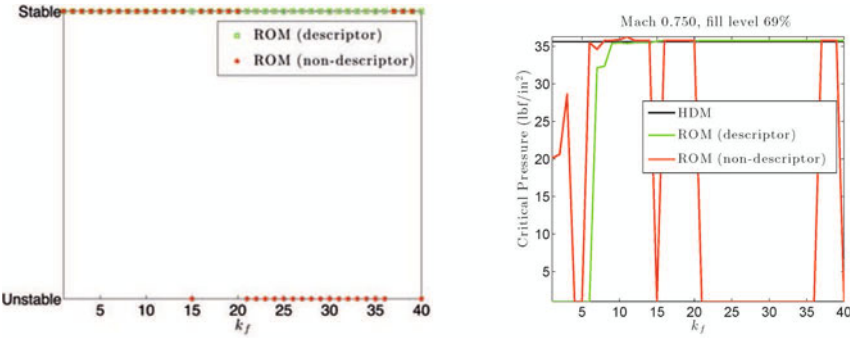

(a) Stability (b) Accuracy

Fig. 8.4. Wing-store-fuel configuration ($M_\infty = 0.75$ and 69% fuel fill level): stability of the fluid ROM as a function of its dimension, and accuracy of the critical free-stream pressure predicted using the corresponding aeroelastic ROM

equispaced reduced frequencies in the interval $[0, 0.04]$: 10 of the computed solution snapshots – more specifically, those associated with the zero reduced frequency – are real-valued, and all other 200 solution snapshots are complex-valued. In other words, the corresponding real-valued matrix $\mathbf{W}$ (8.12) has in this case 410 columns. These are compressed by the POD technique to construct a suite of ROBs and two associated suites of fluid ROMs of dimension $k_f \in \{1, \cdots, 400\}$. The first suite of fluid ROMs is obtained by Galerkin projection of the descriptor form of the LTI fluid subsystem on the computed suite of ROBs. The second one is computed by Galerkin projection of the non-descriptor form of the LTI fluid subsystem on the same suite of ROBs. Then, several instances of the coupled fluid-structure ROM (8.34) are constructed by coupling the modal structural ROM of dimension $k_s = 10$ with each of the computed fluid ROMs.

Fig. 8.5. F18/A configuration at $M_\infty = 0.99$: steady-state surface pressure

First, the stability of the constructed fluid ROMs, and more specifically that of the constructed matrices $\mathbf{H}_r$, is assessed. The obtained results are reported in Fig. 8.6. Once again, all fluid ROMs originating from the descriptor form of the LTI fluid subsystem are found to be stable, but more than half of those originating from its non-descriptor form are found to be unstable.

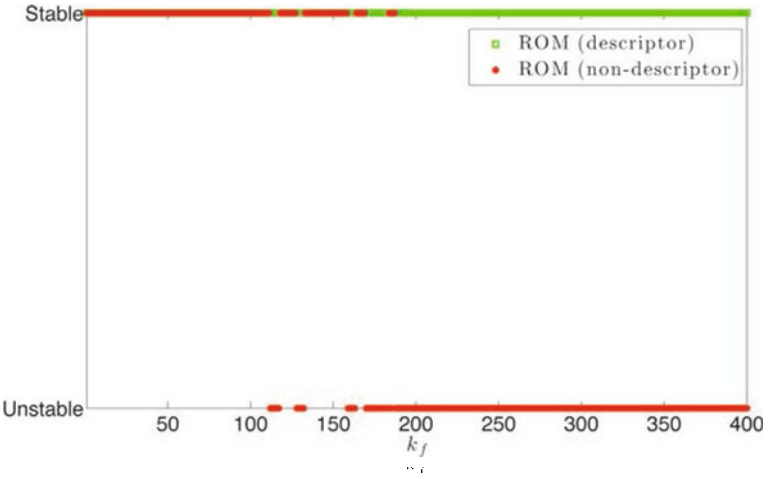

Fig. 8.6. F18/A aeroelastic configuration at $M_\infty = 0.99$: stability of the fluid ROM as a function of its dimension

Next, the accuracy of each constructed aeroelastic ROM is assessed by examining the critical pressure it predicts. The obtained results are reported in Fig. 8.7. From this figure and Fig. 8.6, the reader can observe that every unstable fluid ROM leads to an erroneous prediction of the critical pressure by the corresponding coupled fluid-

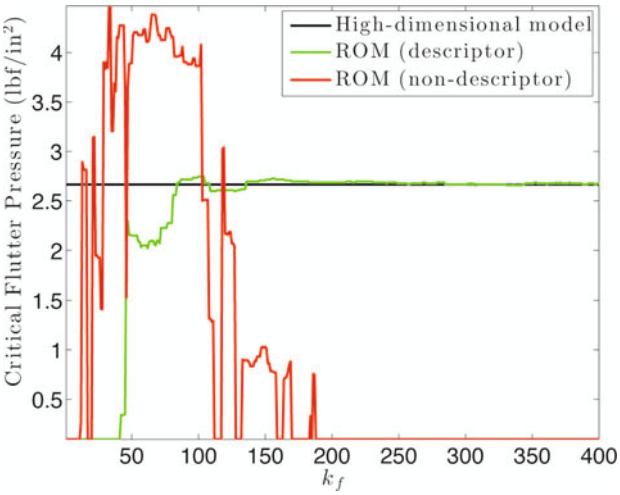

Fig. 8.7. F18/A aeroelastic configuration at $M_\infty = 0.99$: accuracy of the critical free-stream pressure predicted using the aeroelastic ROM

structure ROM. Furthermore, none of the aeroelastic ROMs originating from the non-descriptor form of the fluid LTI subsystem delivers an accurate prediction of the critical pressure. On the other hand, all aeroelastic ROMs originating from this descriptor form and of dimension $k_f \geq 100$ deliver critical pressure predictions that match their HDM counterparts.

8.5 Conclusions

In theory, the Galerkin projection method equipped with Proper Orthogonal Decomposition (POD) modes does not guarantee the stability of the Reduced-Order Models (ROMs) it is often used for constructing. In practice, it is reported in some forums to generate ROMs that are more frequently unstable than stable. Yet, the POD-based Galerkin projection method is among the most popular methods for the dimensional reduction of Linear Time-Invariant (LTI) systems arising from linearized Computational Fluid Dynamics (CFD).

In general, a LTI system can be written in either descriptor or non-descriptor form. The non-descriptor form is characterized by the identity matrix as the coefficient of the highest derivative term in the governing set of Ordinary Differential Equations (ODEs). On the other hand, the leading matrix coefficient of the descriptor form of the same LTI system is usually different from the identity. Therefore, transforming a descriptor form of a given LTI system into its non-descriptor form typically involves pre-multiplying all matrix coefficients of the descriptor form by the inverse of its leading matrix coefficient. Because of the usual numerical issues associated with

computing the inverse of a matrix and/or the solution of potentially ill-conditioned systems of equation, such a transformation could be dismissed *a priori* as a "trouble maker". Nevertheless, such a transformation is routinely performed – and for good reasons – in many computational engineering applications. These range from multibody dynamics [15, 17], to molecular dynamics [26], to CFD [2, 7, 16, 20, 23]. For example, the *nonlinear* semi-discrete equations of dynamic equilibrium governing a flow problem are often transformed from their descriptor form to their non-descriptor form, in order to improve accuracy and accelerate convergence. Indeed, the leading matrix coefficient of the governing set of nonlinear ODEs governing a CFD problem is usually a diagonal matrix storing the volumes of the mesh cells when semi-discretization is performed using a finite volume method, or the volumes of the mesh elements when semi-discretization is performed using a finite element method. Hence, in this case, transforming the descriptor form of the governing set of nonlinear ODEs into its non-descriptor counterpart is a trivial task. It amounts to scaling each entry of the residual vector associated with these equations by the inverse of the corresponding volume of the mesh cell or element. Given that for external flow problems the cells or elements of the mesh are usually very small in the vicinity of the wall boundaries and very large near the far-field artificial boundaries, the non-descriptor form of the governing nonlinear CFD equations magnifies the residuals associated with the small mesh cells or elements. Therefore, the application of a finite number of steps of an iterative procedure to the solution of the non-descriptor form of the governing nonlinear CFD equations delivers a higher accuracy in the flow regions where the mesh cells or elements are the smallest – that is, in the flow regions that matter most – than the application of these same steps to the descriptor form of these equations. Furthermore, when local time-stepping is applied to the solution of a steady-state CFD problem, scaling the residual vector by the inverse of the volumes of the cells or elements of the mesh is often observed to accelerate convergence. For these reasons, many CFD codes effectively operate on the non-descriptor form of the Euler or Navier-Stokes equations. Therefore, it can be conjectured that at least for software legacy reasons, many linearized CFD codes or modules also operate on the non-descriptor forms of the linearized Euler and Navier-Stokes equations. Hence, when model order reduction is or will be implemented in such codes, it is likely to be applied, whether inadvertently or purposely for the reasons outlined above, to the non-descriptor form of the governing ODEs. This conjecture is supported by references such as [2, 7, 16, 20, 23] and others.

In this paper however, it was shown that whereas the snapshot solutions computed using either the descriptor or non-descriptor form of a CFD-based LTI system are identical, the ROMs obtained by reducing both forms of this system using a Galerkin projection method are different. More importantly, using as background the field of linearized computational aeroelasticity, it was also shown numerically that in general, the fluid ROMs constructed by applying the POD-based Galerkin projection method to the non-descriptor form of a CFD-based LTI subsystem of interest are more often unstable then stable. It was also shown that the stability of these ROMs is very sensitive to their dimension. This is consistent with the observations frequently reported in various forums about the inconsistent behavior of POD as far as stability

is concerned. On the other hand, it was also shown numerically that for the same aeroelastic problems, the fluid ROMs constructed by applying the same POD-based Galerkin projection method to the descriptor form of the CFD-based LTI subsystem of interest are typically stable. Therefore, the findings reported in this paper suggest that when the objective is to construct a CFD-based linear fluid ROM using the POD-based Galerkin projection method, reducing the non-descriptor form of the linearized Euler or Navier-Stokes equations tends to promote the instability of the outcome ROM, whereas reducing the descriptor form of these equations tends to prevent it. Hence, a best practice in implementing the POD-based Galerkin projection method in a given CFD code for the purpose of constructing linear fluid ROMs is to apply this method to the descriptor form of the linearized Euler and Navier-Stokes equations, even when the nonlinear computational modules of this code operate on the non-descriptor form of these equations.

Acknowledgements The authors acknowledge partial support by the Army Research Laboratory through the Army High Performance Computing Research Center under Cooperative Agreement W911NF-07-2-0027, partial support by the Office of Naval Research under Grant N00014-11-1-0707, partial support by a research grant from King Abdulaziz City for Science and Technology (KACST), and partial support by The Boeing Company under Contract Sponsor Ref. 45047. The content of this publication does not necessarily reflect the position or policy of any of these supporters, and no official endorsement should be inferred.

References

1. Amsallem, D., Carlberg, K., Cortial, J., Farhat, C.: A method for interpolating on manifolds structural dynamics reduced-order models. International Journal for Numerical Methods in Engineering **80**, 1241–1258 (2009)
2. Amsallem, D., Farhat, C.: Interpolation method for adapting reduced-order models and application to aeroelasticity. AIAA Journal **46**(7), 1803–1813 (2008)
3. Amsallem, D., Farhat, C.: On the stability of linearized reduced-order models: descriptor vs. non-descriptor form and application to fluid-structure interaction. AIAA Paper 2012-2687, 42nd AIAA Fluid Dynamics Conference and Exhibit. 25–28 June 2012, New Orleans, Louisiana pp. 1–12 (2012)
4. Amsallem, D., Farhat, C.: Stabilization of projection-based reduced-order models. International Journal for Numerical Methods in Engineering **91**, 358–377 (2012)
5. Berkooz, G., Holmes, P., Lumley, J.L.: The proper orthogonal decomposition in the analysis of turbulent flows. Annual Review of Fluid Mechanics **25**, 539–575 (1993)
6. Bond, B.N., Daniel, L.: Guaranteed stable projection-based model reduction for indefinite and unstable linear systems. In: 2008 IEEE/ACM International Conference on Computer-Aided Design (ICCAD), pp. 728–735. IEEE (2008)
7. Chen, G., Sun, J., Li, Y.-M.: Adaptive reduced-order-model-based control-law design for active flutter suppression. Journal of Aircraft **49**(4), 973–980 (2012)
8. Chiu, E., Farhat, C.: Effects of fuel slosh on flutter prediction. AIAA 2009-2682, 50th AIAA/ASME/ASCE/AHS/ASC Structures, Structural Dynamics, and Materials Conference (2009)

9. Degand, C., Farhat, C.: A three-dimensional torsional spring analogy method for unstructured dynamic meshes. Computers and Structures **80**, 305–316 (2002)
10. Dowell, E.H., Thomas, J.P., Hall, K.C.: Transonic limit cycle oscillation analysis using reduced order aerodynamic models. Journal of Fluids and Structures **18**, 17–27 (2004)
11. Epureanu, B.I.: A parametric analysis of reduced order models of viscous flows in turbomachinery. Journal of Fluids and Structures **17**, 971–982 (2003)
12. Farhat, C., Degand, C., Koobus, B., Lesoinne, M.: Torsional springs for two-dimensional dynamic unstructured fluid meshes. Computer Methods in Applied Mechanics and Engineering **163**, 231–245 (1998)
13. Farhat, C., van der Zee, K.G., Geuzaine, P.: Provably time-accurate loosely-coupled solution algorithms for transient nonlinear computational aeroelasticity. Computer Methods in Applied Mechanics and Engineering **195**, 1973–2001 (2006)
14. Hall, K.C., Thomas, J.P., Dowell, E.H.: Proper orthogonal decomposition technique for transonic unsteady aerodynamic flows. AIAA Journal **38**(2), 1853–1862 (2000)
15. Hardt, M., Oskar, V.S.: Dynamic modeling in the simulation, optimization, and control of bipedal and quadrupedal robots. ZAMM, Journal of Applied Mathematics and Mechanics/Zeitschrift für Angewandte Mathematik und Mechanik **83**, 648–662 (2003)
16. Hu, P., Bodson, M., Brenner, M.: Towards real-time simulation of aeroservoelastic dynamics for a flight vehicle from subsonic to hypersonic regime. AIAA 2008-6375, AIAA Atmospheric Flight Mechanics Conference and Exhibit (2008)
17. Jain, A.: Unified formulation of dynamics for serial rigid multibody systems. Journal of Guidance, Control, and Dynamics **14**, 531–542 (1991)
18. Kelley, C.T., Keyes, D.E.: Convergence Analysis of Pseudo-Transient Continuation. SIAM Journal of Numerical Analysis **35**(2), 508–523 (1998)
19. Kim, T.: Frequency-domain Karhunen-Loeve method and its application to linear dynamic systems. AIAA Journal **36**(11), 2117–2123 (1998)
20. Lesoinne, M., Farhat, C.: A CFD based method for solving aeroelastic eigenproblems in the subsonic, transonic, and supersonic regimes. AIAA Journal of Aircraft **38**, 628–635 (2001)
21. Lesoinne, M., Sarkis, M., Hetmaniuk, U., Farhat, C.: A linearized method for the frequency analysis of three-dimensional fluid/structure interaction problems in all flow regimes. Computer Methods in Applied Mechanics and Engineering **190**, 3121–3146 (2001)
22. Lieu, T., Farhat, C.: Adaptation of aeroelastic reduced-order models and application to an F-16 configuration. AIAA Journal **45**(6), 1244–1257 (2007)
23. Lieu, T., Farhat, C., Lesoinne, M.: Reduced-order fluid/structure modeling of a complete aircraft configuration. Computer Methods in Applied Mechanics and Engineering **195**(41–43), 5730–5742 (2009)
24. Luenberger, D.G.: Dynamic equations in descriptor form. IEEE Transactions on Automatic Control, pp. 312–321 (1977)
25. Mortchéléwicz, G.: Aircraft aeroelasticity computed with linearized RANS equations. 43rd Annual Conference on Aerospace Sciences, Tel Aviv, Israel (2003)
26. Nagarajan, V., Jain, A., Goddard, W.: Constant temperature constrained molecular dynamics: The Newton-Euler inverse mass operator method. The Journal of Physical Chemistry **100**, 10,508–10,517 (1996)
27. Sirovich, L.: Turbulence and the dynamics of coherent structures. Part I: Coherent structures. Quarterly of Applied Mathematics **45**(3), 561–571 (1987)
28. Thomas, J.P., Dowell, E.H., Hall, K.C.: Nonlinear inviscid aerodynamic effects on transonic divergence, flutter, and limit-cycle oscillations. AIAA Journal **40**, 638–646 (2002)

29. Thomas, J.P., Dowell, E.H., Hall, K.C.: Three-dimensional transonic aeroelasticity using proper orthogonal decomposition-based reduced order models. Journal of Aircraft **40**(3), 544–551 (2003)
30. Willcox, K., Peraire, J.: Balanced model reduction via the proper orthogonal decomposition. AIAA Journal **40**(11), 2323–2330 (2002)